The Genomic Landscapes of Desert Birds Form over Multiple Time Scales

Kaiya Provost *[,1,2,3,4,5] Stephanie Yun Shue,[4,5] Meghan Forcellati,[4,6] and Brian Tilston Smith[1]

[1]Department of Ornithology, American Museum of Natural History, New York, NY, USA
[2]Richard Gilder Graduate School, American Museum of Natural History, New York, NY, USA
[3]Department of Evolution, Ecology and Organismal Biology, The Ohio State University, Columbus, OH, USA
[4]Bergen County Academies, Hackensack, NJ, USA
[5]Biological Sciences, University of California Berkeley, Berkeley, CA, USA
[6]Ecology, Evolution, and Environmental Biology, Columbia University, New York, NY, USA

***Corresponding author:** E-mail: provost.27@osu.edu.

Associate editor: Dr. Anne Yoder

Abstract

Spatial models show that genetic differentiation between populations can be explained by factors ranging from geographic distance to environmental resistance across the landscape. However, genomes exhibit a landscape of differentiation, indicating that multiple processes may mediate divergence in different portions of the genome. We tested this idea by comparing alternative geographic predctors of differentiation in ten bird species that co-occur in Sonoran and Chihuahuan Deserts of North America. Using population-level genomic data, we described the genomic landscapes across species and modeled conditions that represented historical and contemporary mechanisms. The characteristics of genomic landscapes differed across species, influenced by varying levels of population structuring and admixture between deserts, and the best-fit models contrasted between the whole genome and partitions along the genome. Both historical and contemporary mechanisms were important in explaining genetic distance, but particularly past and current environments, suggesting that genomic evolution was modulated by climate and habitat There were also different best-ftit models across genomic partitions of the data, indicating that these regions capture different evolutionary histories. These results show that the genomic landscape of differentiation can be associated with alternative geographic factors operating on different portions of the genome, which reflect how heterogeneous patterns of genetic differentiation can evolve across species and genomes.

Key words: **genomics, isolation by distance, genomic landscapes, isolation by ecology, model selection, divergence.**

Introduction

Levels of nucleotide diversity and the degree of differentiation both vary across genomes (e.g., Ellegren et al. 2012; Li and Ralph 2019). These so-called genomic landscapes are produced by variable processes including ones intrinsic to the genome (meiotic recombination, mutation) and those extrinsic (introgression, selection, and drift). Fluctuating levels of genetic diversity across the genome have been shown to be associated with recombination rate indicating that linked selection reduces variation (Burri et al. 2015; Martin and Jiggins 2017; Johri et al. 2020). Likewise mutation rates and coalescent times are all known to covary with levels of differentiation across the genome (Benzer 1961; Hodgkinson and Eyre-Walker 2011; Nosil and Schluter 2011). In contrast to intrinsic processes which are primarily mediated by genomic properties, extrinsic processes are mediated through interactions with the adaptive and demographic factors operating across space. The locations of speciation genes are found to be associated with genomic differentiation (Benzer 1961; Hodgkinson and Eyre-Walker 2011; Nosil and Schluter 2011). Despite evidence of the patterns and processes driving a heterogeneous genomic landscape (e.g., Li and Ralph 2019; Wang et al. 2020), studies examining the geographic predictors of genetic differentiation often use only single summary statistics to represent the entirety of the genome, for example using a single F_{ST} value for comparing whole populations. Clarifying the relationship between the heterogeneity of the genomic landscape and geographic predictors of differentiation will elucidate how intraspecific variation arises in the complex physical landscape.

The spatial processes attributed to population differentiation operate over historical through contemporary time scales; herein, we focus on five as examples. An atemporal manifestation of historical isolation, such as isolation by barrier(s) (IBB; *sensu* Mayr 1942) can occur, where population differentiation is best predicted by a landscape feature. Over shallower evolutionary scales, nonrandom mating with individuals in closer geographic proximity can cause genetic differentiation by isolation by distance (IBD; Wright

Article

1943). IBD has been shown to impact taxa at both small (e.g., Aguillon et al. 2017) and large geographic scales (e.g., Reletheford 2004). Geographic distances alone may not be the best predictors of differentiation because adaptation to local climatic conditions causes selection to generate structuring across environmental gradients, which is known as isolation by environment (IBE; Wang and Bradburd 2014; Berg et al. 2015; Zamudio et al. 2016; Myers et al. 2019). These two factors have been shown to work concurrently with one another in many groups (Sexton et al. 2014). Because local environmental conditions change rapidly, for example due to species turnover or succession (Phillips 1996; Nuvoloni et al. 2016), associations between differentiation and environment are likely more recent phenomena than historical associations. The increased availability of ecological data for many organisms, such as census data, allows for testing even shallower associations with genetic structuring across the landscape. Contemporary demographic data can be used to test whether genetic differences are associated with abundance troughs that restrict gene flow (Barton and Hewitt 1981; Hewitt 1989; Barrowclough et al. 2005; referred to herein as "IBA" for brevity). Though it is often assumed that abundance and niche occupancy are correlated due to the link with suitable habitat (Holt 2009), this is not necessarily borne out (Waldock et al. 2022) and as such we estimate these factors separately. Local population size is also known to be a strong driver of genetic structure, especially when compounded with environmental change determining local suitability (Weckworth et al. 2013). Finally, population history is often linked to Pleistocene glacial cycles that shifted and fragmented distributions. An association of genome-wide structuring linked to population fragmentation can be tested under a scenario where genetic distances are modeled against paleo-climatic suitability (Vasconcellos et al. 2019; Moreira et al. 2020; referred to herein as "IBH" for brevity).

While the focus of these models is often on genetic variation, they can also be applied to phenotypic variation (e.g., Moreira et al. 2020). Phenotypic variation is often the product of many loci with little effect (Zeng 1994). As such, looking directly at phenotype can help reveal whether a particular process is associated with trait variance. Examining the genomic landscape in the context of these alternative geographic models will provide evidence for how factors of varying temporal resolutions influence the peaks and valleys of differentiation. To investigate how landscape features impact genotypic and phenotypic variation across space, we use an archetypical assemblage of co-distributed birds distributed across the Sonoran and Chihuahuan Deserts of the southwestern USA and northern Mexico.

Here, we characterize the genomic landscapes of birds occurring across the Sonoran and Chihuahuan Deserts and test the relative effect of alternative geographic models in predicting patterns of intraspecific differentiation. To do this, we integrate population-level whole-genome resequencing, specimen-based morphometrics, and comparative sampling across ten co-distributed species that occur across the deserts. We hypothesize that the best-predictors of genetic diversity will vary across species and different partitions of the data, reflecting the multiple extrinsic factors that structure variation across the genomic landscape (supplementary fig. S1, Supplementary Material online). Alternatively, species could show homogeneous patterns either by the same geographic modeling predicting differentiation in windows across the whole genome or by species exhibiting congruent genomic landscapes shaped by the same geographic barrier. We further evaluate whether summary statistics, reflective of alternative evolutionary processes, could explain alternative geographic predictors of genomic landscapes. This comparative framework will provide resolution to the extent at which peaks and valleys of the genomic landscape correspond to historical through contemporary factors.

Results

Summary of Genomic Data

We sequenced the genomes of 221 individuals across 10 focal species of passerine birds distributed in the Sonoran and Chihuahuan Deserts (fig. 1). Individuals varied in their coverage across the genome. We created three datasets to address this variation in downstream analyses: a complete dataset of all individuals, a dataset where individuals with greater than 75% missing base pairs were removed, and a dataset where individuals with greater than 50% missing base pairs were removed; we call these the 100%, 75%, and 50% missing data partitions, respectively. We found that the three missing data partitions did not vary substantially with respect to coverage at non-missing sites or number of SNPs. As such, here we describe the results for the complete dataset (for the 75% and 50% missing data partitions, see supplementary information, Supplementary Material online). We recovered sequences with a mean coverage of 2.9 per individual (range 0.4–8.8), 6–25 million reads per individual, and 5–28 million SNPs per species. Mean × coverage within species ranged from

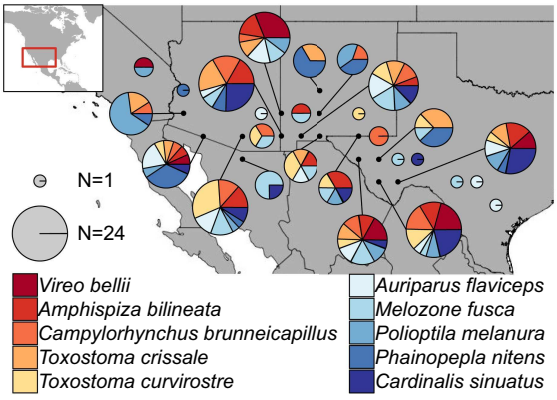

FIG. 1. Sampling map of study. Localities are given with points (with latitudes/longitudes of specimens rounded to nearest degree). Pie charts show the number (radius of pie chart) and species identity (slices) of specimens used from that area. Large pie charts are linked to their locality with a line.

Table 1. Chromosome-Wise Values for the Recombination Rate, F_{ST}, D_{XY}, and Proportion of Missing Data Per Each Species.

Species	Rec ($\times 10^{-10}$)	F_{ST}	D_{XY}	% missing sites
Vireo bellii	9.7 ± 1.2 (33)	0.06 ± 0.09 (35)	0.011 ± 0.005 (31)	0.64 ± 0.79 (36)
Amphispiza bilineata	11.1 ± 0.5 (35)	0.02 ± 0.001 (35)	0.018 ± 0.005 (20)	0.55 ± 0.43 (36)
Campylorhynchus brunneicapillus	10.4 ± 0.3 (31)	0.03 ± 0.001 (34)	0.011 ± 0.008 (31)	0.55 ± 0.02 (36)
Toxostoma crissale	10.5 ± 0.4 (31)	0.04 ± 0.004 (34)	0.01 ± 0.006 (31)	0.52 ± 0.41 (36)
Toxostoma curvirostre	10.0 ± 0.5 (34)	0.10 ± 0.023 (34)	0.013 ± 0.009 (32)	0.52 ± 0.41 (36)
Auriparus flaviceps	10.2 ± 0.7 (34)	0.05 ± 0.006 (36)	0.015 ± 0.007 (35)	0.56 ± 0.47 (36)
Melozone fusca	10.1 ± 0.5 (35)	0.04 ± 0.004 (35)	0.015 ± 0.01 (24)	0.51 ± 0.47 (36)
Polioptila melanura	9.7 ± 0.7 (29)	0.03 ± 0.001 (34)	0.014 ± 0.01 (23)	0.52 ± 0.43 (36)
Phainopepla nitens	10.0 ± 0.6 (30)	0.02 ± 0.001 (34)	0.012 ± 0.007 (28)	0.65 ± 0.01 (36)
Cardinalis sinuatus	9.8 ± 0.6 (36)	0.03 ± 0.005 (36)	0.015 ± 0.01 (26)	0.52 ± 0.35 (36)

NOTE.—Values given as mean ± standard deviation (number of chromosomes). These are calculated by weighting all chromosome means equally; for size-weighted values, see supplementary table S1, Supplementary Material online. Note that the number of chromosomes was based on the pseudo-chromosomes we generated, with a maximum of 36. "Rec" = population recombination rate, or rho. Values are given for the complete dataset; for the 50% and 75% values, see supplementary table S1, Supplementary Material online.

2.1× to 4.2×, with *Phainopepla nitens* having the lowest coverage and *Melozone fusca* the highest. The average missing data per species ranged from 48% to 64%. Across individuals, missing data ranged from 13% to 93% with a mean of 53% (table 1; supplementary figs. S12-S13, Supplementary Material online).

Recombination Rate

Mean recombination rates for the entire genome estimated using ReLERNN (Adrion et al. 2020) ranged from 8.9 to 12.8×10^{-10} c/bp (where c is the probability of a crossover) across species. Correlations between species in mean recombination across chromosomes ranged from −0.57 to 0.53 (mean ± SD 0.02 ± 0.25). Correlations between species in mean recombination at the same genomic positions ranged from −0.33 to 0.43 (mean ± SD −0.01 ± 0.22). Recombination rate was not associated with log-corrected chromosome size ($P = 0.82$).

Lostruct Outliers and F_{ST} Outliers

We divided the genome into three kinds of partitions. First, we analyzed chromosomes independently. Second, we identified high-F_{ST} outliers (by calculating the *z*-score of F_{ST} values across the genome within species and retaining only those more than 5 standard deviations above the mean) and analyzed those. Finally, we performed a multidimensional scaling (MSDS) analysis the using R package lostruct version 0.0.0.9000 (Li and Ralph 2019), which subdivided genomes into four partitions, three outliers (LS1, LS2, LS3), and one nonoutlier partition (fig. 2; supplementary fig. S2, Supplementary Material online). Note that outlier groupings are not analogous across taxa. On average, across all species 85.3% of labeled values were nonoutliers, and ∼4.88% each were LS1, LS2, and LS3.

The number of highly differentiated regions in the genome varied between species. F_{ST} outlier analysis across datasets with different levels of missing data found largely congruent results with respect to how many outliers were present across taxa (see supplementary information, Supplementary Material online for 75% and 50% datasets). The number of high-F_{ST} outliers for the complete dataset ranged from 28 to 758 across species (with the total number of windows analyzed per species ranging from 100,733 to 113,555). The outlier lostruct partitions identified above (LS1, LS2, LS3) vary in the proportion of the F_{ST} outliers examined (for the complete dataset), ranging from 0.0% to 3.4% (mean 0.2%) for peaks. Though not significant, there appears to be a trend where species with generally higher F_{ST} have more high-F_{ST} outliers identified.

Population Differentiation

Signatures of population structure varied in our ten species. Population differentiation in species ranged from being highly structured among deserts in four species (*T. curvirostre*, *V. bellii*, *A. flaviceps*, and *P. melanura*), showing a gradient of structuring with admixture in three (*T. crissale*, *M. fusca*, and *Cardinalis sinuatus*), or unstructured in the remaining taxa (*A. bilineata*, *C. brunneicapillus*, *P. nitens*; supplementary fig. S3, Supplementary Material online; supplementary fig. S16, Supplementary Material online; supplementary fig. 17, Supplementary Material online; supplementary fig. 18, Supplementary Material online). F_{ST} values for the species within these three groups varied accordingly: highly structured = 0.03–0.10; gradient = 0.03–0.04; and unstructured = 0.02–0.03. Population differentiation estimated from the chromosomal partitions were generally concordant with genome-level patterns, but smaller chromosomes and/or those with fewer SNPs showed different patterns (figs. 3 and 4; supplementary fig. S4, Supplementary Material online; supplementary fig. S23; Supplementary Material online; supplementary fig. S24; Supplementary Material online).

Species varied in how wide their clines of genetic relatedness were between chromosomes. Mean cline width ranged from 6.9° to 15.9° longitude, where the total area encompassed by each species was ∼18° longitude (with zero on the cline defined as 116.1°W longitude; supplementary table S2, Supplementary Material online; figs. 3 and 4; supplementary fig. S1, Supplementary Material online). Cline width increases as chromosome size decreases ($P = 1.4 \times 10^{-6}$, adjusted $R^2 = 0.06$), though this varies across species (range $P = 7.7 \times 10^{-7}$–0.43, range adjusted $R^2 =$ −0.01 to 0.51). Mean cline center location ranges from

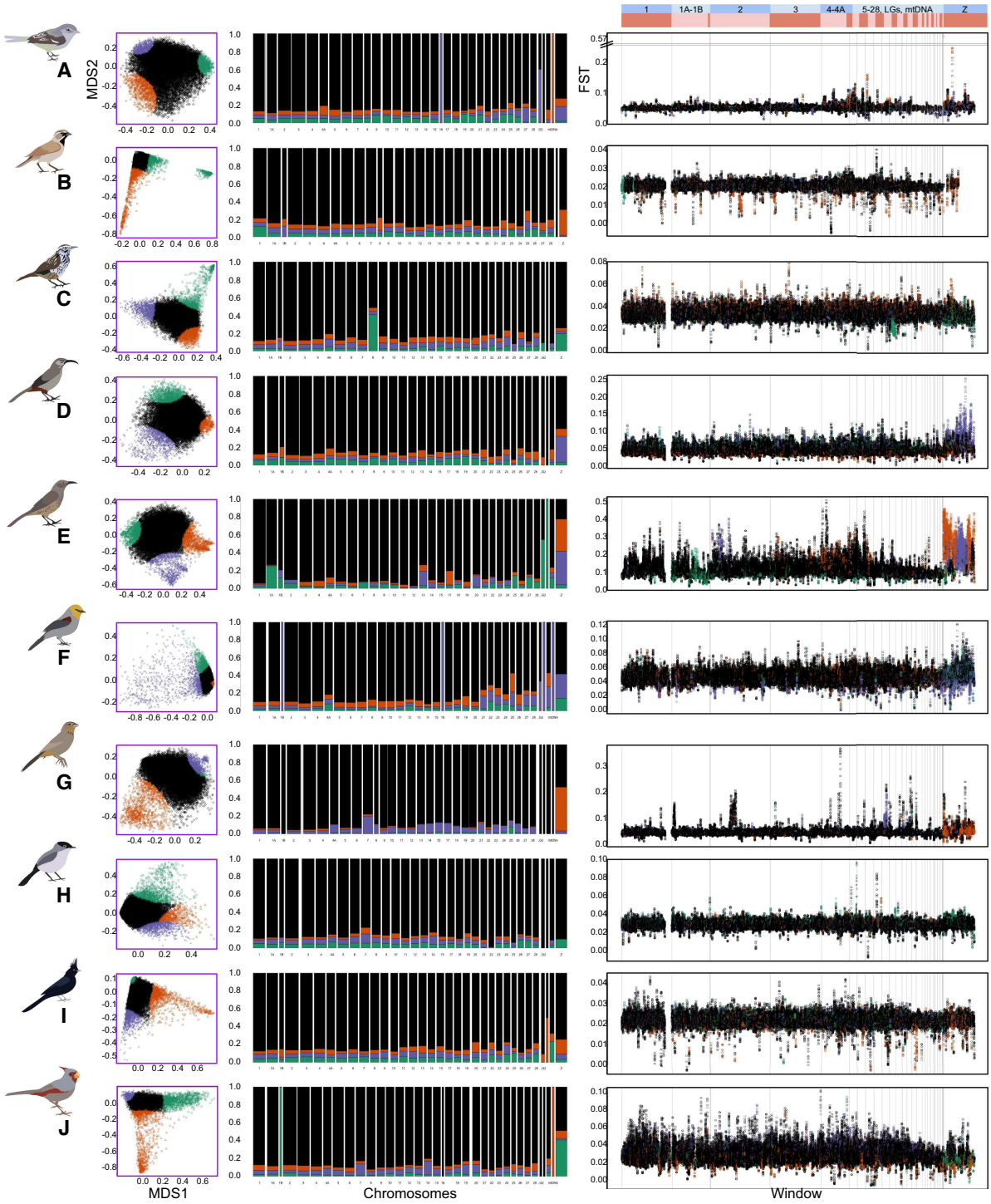

Fig. 2. Lostructpartitions vary across species and across chromosomes. Species are as follows: (*A*) *Vireo bellii*, (*B*) *Amphispiza bilineata*, (*C*) *Campylorhynchus brunneicapillus*, (*D*) *Toxostoma crissale*, (*E*) *Toxostoma curvirostre*, (*F*) *Auriparus flaviceps*, (*G*) *Melozone fusca*, (*H*) *Polioptila melanura*, (*I*) *Phainopepla nitens*, (*J*) *Cardinalis sinuatus*. Left column: Multidimensional scaling coordinate 1 (*x*-axis) versus 2 (*y*-axis) for each species, with outlier points highlighted in orange, green, and purple as different partitions, and nonoutlier points in black. Middle column: proportion of chromosomes assigned to LS1 (orange), LS2 (green), LS3 (purple), and nonoutlier (black) lostruct partitions. Width of bars approximately proportional to length of each chromosome. Right column: F_{ST} values for windows across the genome, colored by lostruct partition (orange, green, purple, black). Each window represents one 100,000 base pair wide section of the genome, with subsequent windows overlapping by 10,000 base pairs. Note that F_{ST} values are not on the same scale for all taxa. Chromosomes separated by lines, with legend at the top. Species images are not to scale. For references to color see the online version.

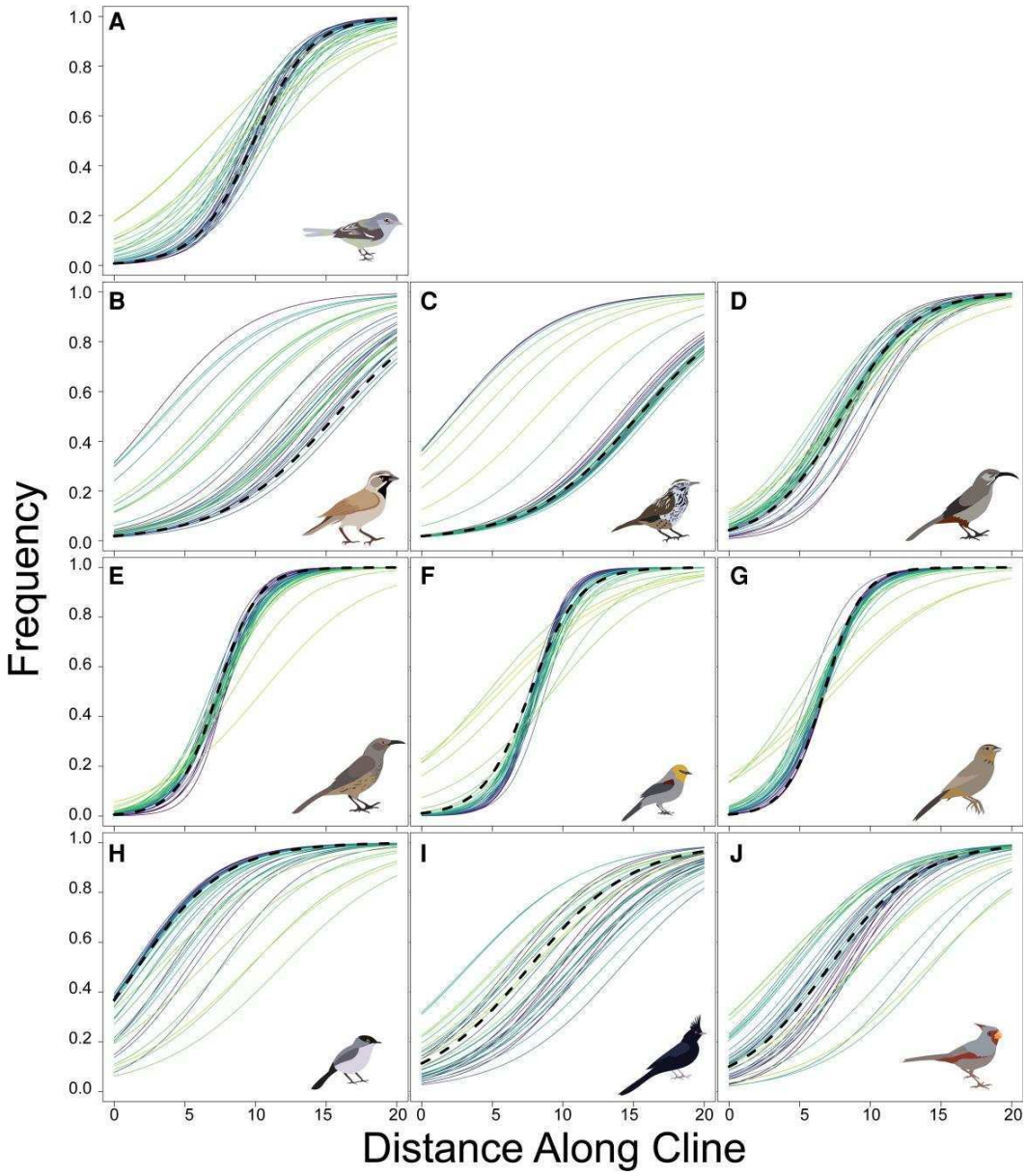

Fig. 3. Cline width and center location vary across species and across chromosomes. *X*-axis shows distance (in degrees longitude) along the sampled area. *Y*-axis shows the projected cline from population assignments of 0–1 in each taxon (panel) and each chromosome (lines). Genomes are given by thick dashed lines. Species are as follows: (*A*) *Vireo bellii*, (*B*) *Amphispiza bilineata*, (*C*) *Campylorhynchus brunneicapillus*, (*D*) *Toxostoma crissale*, (*E*) *Toxostoma curvirostre*, (*F*) *Auriparus flaviceps*, (*G*) *Melozone fusca*, (*H*) *Polioptila melanura*, (*I*) *Phainopepla nitens*, (*J*) *Cardinalis sinuatus*. Species images are not to scale.

3.6° along the cline (~112°W) to 12.7° along the cline (~103°W). We found that there were negative correlations between the degree of population structure (measured by F_{ST}; see supplementary information, Supplementary Material online) and both mean cline width and the standard deviation of cline center locations, which was expected based on how clines are calculated. Species with higher F_{ST} between populations had narrower clines and less variation among partitions in the locations of their clines (supplementary fig. S5, Supplementary Material online). Cline width is also significantly, but weakly, associated with recombination rate ($P = 0.0023$, adjusted $R^2 = 0.02$)

Phenotypic Variation across the Cochise Filter Barrier

There were no clear, desert-specific patterns in morphological variation across the Cochise Filter Barrier ($N = 234$), with morphological changes ranging from subtle to significantly different. In our principal components analysis, the first three principal components (PC1, PC2, PC3) explained 74%, 12%, and 6% of the variation in morphology and

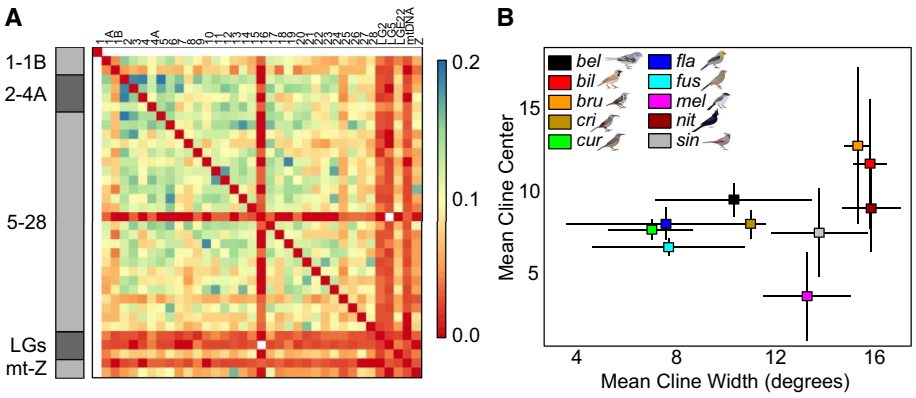

Fig. 4. Species varied both in genetic structure across chromosomes and population structure across the Sonoran and Chihuahuan Deserts. (*A*) Standard deviations of normalized Robinson–Foulds distances, averaged across species; see supplementary figure S4, Supplementary Material online. Warmer values indicate lower standard deviations and less variation across taxa. Chromosomes are arranged in alphanumeric order; *y*-axis shows blocks of chromosomes for legibility, *x*-axis shows individual chromosomes. (*B*) Mean cline width in degrees versus mean cline center across chromosomes for each species; see figure 3. Lines from each point show standard deviations. Species names are shortened for legibility ("bel" = *Vireo bellii*, "bil" = *Amphispiza bilineata*, "bru" = *Campylorhynchus brunneicapillus*, "cri" = *Toxostoma crissale*, "cur" = *Toxostoma curvirostre*, "fla" = *Auriparus flaviceps*, "fus" = *Melozone fusca*, "mel" = *Polioptila melanura*, "nit" = *Phainopepla nitens*, "sin" = *Cardinalis sinuatus*).

corresponded approximately to overall body size, bill size/shape, and wing size/shape, respectively (supplementary tables S3 and S4 and fig. S9, Supplementary Material online). We found significant differences across the Cochise Filter Barrier in six species in at least one analysis (fig. 6; see supplementary information, Supplementary Material online for more details). Between deserts, *T. crissale* and *C. sinuatus* differed in body size and bill shape. *Vireo bellii* and *M. fusca* differed in bill shape. *Polioptila melanura* and *A. flaviceps* differed in body size. No species showed significant differences in wing shape.

Climatic Suitability and Abundance across the Cochise Filter Barrier

During the Last Glacial Maximum, the most suitable areas for all taxa were projected to be further south than the most suitable areas during the present and mid-Holocene. Regions that are predicted to be suitable through all three periods are often reduced compared to current distributions (supplementary figs. S8 and S10, Supplementary Material online). We calculated abundance for each species using the Breeding Bird Survey (Pardieck et al. 2019). Abundance was correlated with predicted climatic suitability across all taxa, with adjusted R^2 values of fit lines (log-scaled) ranging from 0.42 to 0.62 (fig. 4; supplementary figs. S6 and S7, Supplementary Material online).

Phenotypic and Genotypic Datasets Are Idiosyncratic with Respect to Landscape Features

We used generalized dissimilarity matrix (GDM) models to determine which geographic features best described variation in different partitions of genetic and phenotypic data. We had 515 combinations of species and partitions (out of a total possible of 540). For univariate models, performance of GDM models was generally consistent whether looking at univariate, bivariate, or trivariate data partitions (see supplementary information, Supplementary Material online). 2,899/3,090 univariate models converged successfully with an overall 94% convergence. Of those 515 datasets tested, 18.0% selected IBE as the best factor explaining variation, 17.5% selected IBB, 17.2% selected IBA, 9.1% selected IBD, 18.8% selected IBH, and the remainder was ambiguous, with multiple models equally explaining variation. Within the ambiguous models, of which there were 98, the best models often included IBE (99.0% of models), IBH (81.6%), and IBD (72.5%); in contrast, the best models rarely included IBA (4.1%) or IBB (2.0%). Across all the GDMs, percent deviance explained by the best model was variable, ranging from 0.1% to 81.9%. The mean ± SD percent deviance explained for these runs was 12.7% ± 13.6%. Percent deviance explained for the whole genome was lower on average, ranging from 0.1% to 29.2% (mean ± SD 10.8% ± 10.4%). F_{ST} outliers, both high and low, tended to have lower percent deviances explained, ranging from 0.1% to 21.9% (mean ± SD 6.5%±6.5%). Lostruct outliers ranged from 0.5% to 32.2% (mean ± SD 8.1% ± 7.3%). Percent deviance explained had the most extreme range in morphology, from 0.3% to 81.9% (mean ± SD 16.6%±20.8%). The percent deviance explained for all datasets varied across taxa, with means ranging from 3.2% (*M. fusca*) to 20.3% (*A. bilineata*) and standard deviations ranging from 8.7% to 16.4%.

For the models examining signals across the whole genomes, three species had IBB as the most important predictor, one had IBE, two had IBH, one had IBA, and three had mixed support (fig. 5; supplementary fig. S11, Supplementary Material online). IBD was the least common predictor across chromosomes (5.2%), while all

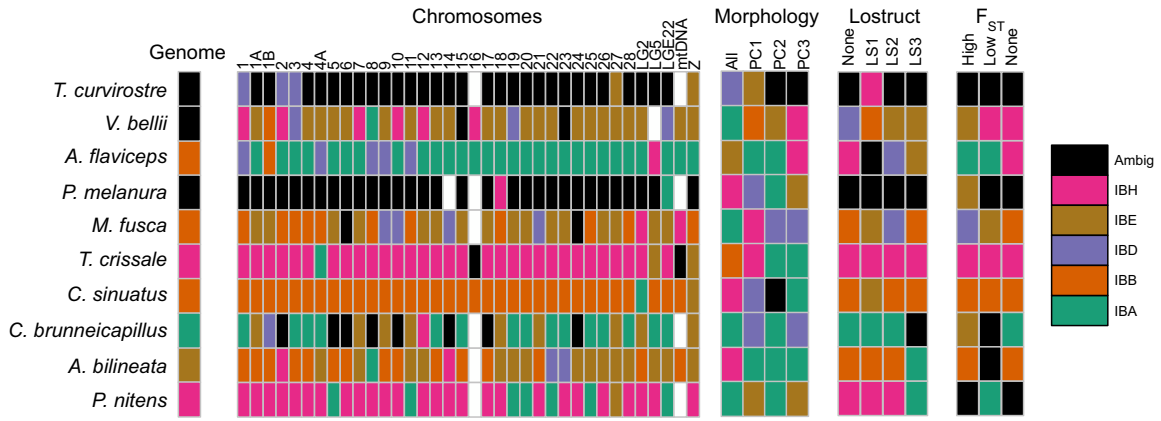

Fig. 5. Generalized Dissimilarity Modeling revealed heterogeneous associations between genomic and phenotypic differentiation and alternative geographic hypothesis. Shown are the best-performing GDM across all univariate, bivariate, and trivariate models. Species are along the *y*-axis and arranged from most to least differentiated across the Cochise Filter Barrier. Individual partitions are along the *x*-axis (whole genome, individual chromosomes, morphology, lostruct partitions, F_{ST} outliers). "Genome" refers to a partition where all genomic information was assessed at once. The alternative models were as follows: isolation by abundance (IBA), isolation by barrier (IBB), isolation by distance (IBD), isolation by environment (IBE), and isolation by history (IBH). "Ambig" is shorthand for ambiguous partitions where multiple models equally best explain the data. Empty boxes represent models that failed to converge or did not have corresponding datasets. For more partitions of data, see supplementary figures S2 and S11, Supplementary Material online.

other predictors were of approximately equal frequency (19.6% IBH, 19.0% IBE, 18.2% IBB, 17.0% IBA, and 20.8% mixed support for multiple models). Within the mixed models, IBE was included 100% of the time, IBH was included 77.7% of the time, IBD was included 73.6% of the time, and IBE and IBB were each included 2.3% of the time.

For the lostruct partitions, the outlier partitions (LS1, LS2, LS3) had 4/30 with IBA as the best model, 6/30 IBB, 2/30 IBD, 5/30 IBE, 6/30 IBH, and 7/30 as ambiguous. Among the ambiguous models, all of them showed IBE as important and nearly all showed IBH, IBD, or both as important. Most species showed at least some overlap in which model best explained partitions: for example, *A. bilineata* and *C. sinuatus* all have at least two lostruct partitions best explained by IBB.

For the nonoutlier partitions (LS0), the best model chosen was the same as the best model explaining whole-genome variation in all but three species (*V. bellii*, *A. flaviceps*, and *A. bilineata*) and that of one of the outlier partitions in all but two species (*V. bellii* and *A. flaviceps*). Notably, for *P. melanura* all three outlier partitions, the genome, and the nonoutlier lostruct partitions are explained by multiple models (specifically, IBD, IBE, and IBH for all). Likewise, for *T. crissale*, all of these were explained by IBH.

For the genomic regions with F_{ST} outliers, the best predictors across species were generally congruent between different outlier partitions and the whole genome. In all species but *A. bilineata*, the non-F_{ST} outliers had the exact same best predictors as that of the whole genome (or in cases where multiple models were equally good predictors, one was a subset of the other). High-F_{ST} outliers showed different best predictors than the genome in *C. brunneicapillus*, *A. bilineata*, *A. flaviceps*, and *M. fusca*. Low-F_{ST} outliers showed different best predictors than the genome in *C. brunneicapillus*, *A. flaviceps*, *M. fusca*, and *P. nitens*.

There was little congruence across the best landscape predictor of morphological data within species; however, the best-performing model across these three datasets was most frequently IBA (37.5%), IBD (17.5%), and IBH (17.5%), with relatively fewer models with IBE (12.5%), IBB (7.5%), IBB or a mixture of models (7.5%, with approximately even amounts of IBA, IBD, IBE, and IBH making up the mixture). 3/30 of the PCs matched overall morphology in terms of best predictors (including mixtures of models). Additionally, 10/30 individual PCs did match each other when they did not match the genome: PC1 and PC2 in four species, PC1 and PC3 in two species, and PC2 and PC3 in four species. Notably, all PCs in *A. bilineata* were best explained by IBA despite its overall morphology being best explained by IBH. While the distribution of best models for overall morphology, PC1, and PC3 were not significantly different than expected, for PC2 this was nearly significant ($\chi^2 = 6.8$, $P = 0.079$, df = 3, simulated $P = 0.11$)

Overall morphological variation was best explained by IBA in 4/10 species, IBH in 3/10, and 1/10 each for IBB, IBD, and IBE, respectively. In contrast, PC1 (body size) showed a more even distribution between all models (1/10 IBE, 2/10 IBA, 3/10 IBD, 2/10 IBB, and 2/10 IBH). PC2 (bill shape) was best explained in 6/10 of species by IBA, 1/10 each by IBE and IBD, and 2/10 with a mixture of results (combinations of IBA, IBD, IBH, and IBE). Lastly, PC3 (wing shape) was best explained in 3/10 of species by IBA, 2/10 each by IBE, IBD, and IBH, and 1/10 of species had ambiguous results (IBA, IBE, and IBH).

Data Characteristics of Best-Fit Models

Genomic summary statistics were associated with which geographic patterns best predicted variation within species. Cline width per chromosome was significantly

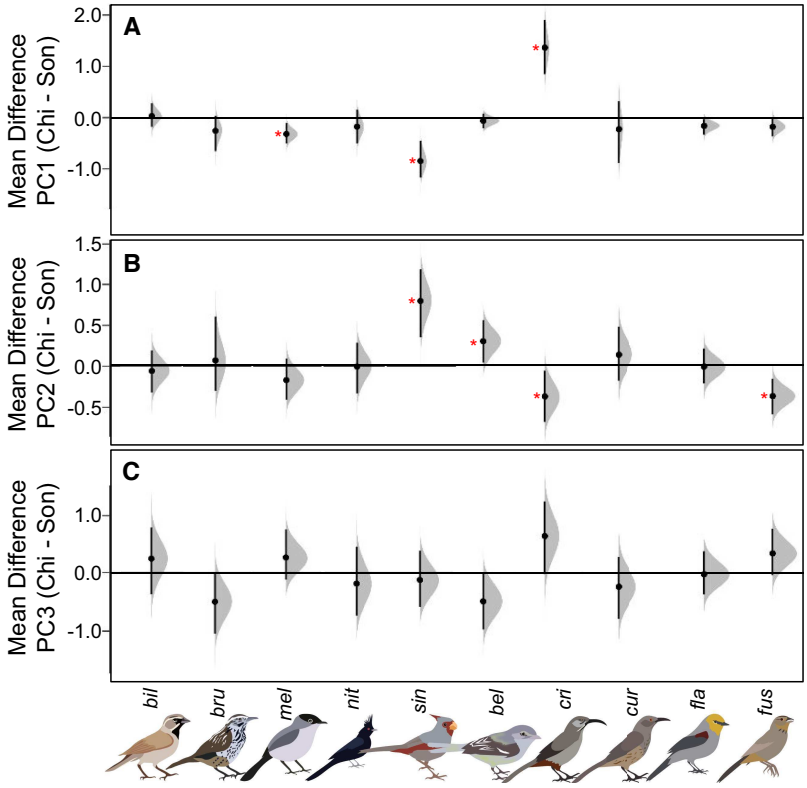

Fig. 6. Distribution of unpaired mean differences between Sonoran and Chihuahuan Desert individuals for each species from DABEST analysis for morphological PC1 (*A*), PC2 (*B*), and PC3 (*C*). Horizontal line is at zero, points and vertical lines show mean and confidence intervals for each distribution. Comparisons that do not cross zero are considered significant in DABEST tests, indicated with asterisk. On the *X*-axis are each species with images (scale does not reflect size differences) with species names are shortened for legibility ("bel" = *Vireo bellii*, "bil" = *Amphispiza bilineata*, "bru" = *Campylorhynchus brunneicapillus*, "cri" = *Toxostoma crissale*, "cur" = *Toxostoma curvirostre*, "fla" = *Auriparus flaviceps*, "fus" = *Melozone fusca*, "mel" = *Polioptila melanura*, "nit" = *Phainopepla nitens*, "sin" = *Cardinalis sinuatus*).

different relative to the predictors ($P = 1.85\times10^{-5}$), being wider between IBB models and IBD or mixed models, between IBH models and IBD or mixed models, and between IBE and IBD models. Cline centers also significantly differed, with chromosomes supporting mixed models having much more eastern cline centers than chromosomes supporting IBA, IBB, IBE, or IBH models. Centers were also significantly more eastern for chromosomes predicted by IBA models than by IBH models ($P = 8.86\times10^{-10}$). Chromosomes with lower recombination were significantly more likely to be explained by mixed models than by IBA or IBE models ($P = 0.0147$). Chromosomes explained by mixed models also had higher estimated F_{ST} than those explained by IBA, IBB, or IBH models ($P = 4.2\times10^{-5}$). Chromosomes with IBH as the best model had lower D_{XY} than those with IBB or IBE as best models. Chromosomes with less missing data were more likely to show mixed support for models compared to IBA, IBE, or IBH models, and more likely to show IBB over IBA or IBE models. Species with higher mean contact zone suitability were more likely to have IBB as the best model compared to all other models, and species with lower contact zone suitability were more likely to have IBH as the best model compared to all other models. Likewise, species with highly variable habitat suitability were more likely to have IBH as the best model. Not significant at all was chromosome length across predictors. Tajima's D was significantly different across chromosomes with different models ($P = 0.0432$), but Tukey's honestly significant difference tests showed that none of the individual comparisons were significant.

Species differed more than expected with respect to what geographic models best explain their genotypes and phenotypes. Best-predictors vary across individual species ($\chi^2 = 816.8$, $P \sim 0.0$, df = 45, simulated $P < 0.0005$) and with respect to whether or not species have phylogeographic structure across the Cochise Filter Barrier ($\chi^2 = 188.6$, $P \sim 0.0$, df = 10, simulated $P < 0.0005$). However, best-predictors did not vary with respect to individual genotypic or phenotypic partitions ($\chi^2 = 238.3$, $P = 0.88$, df = 265, simulated $P = 0.88$; supplementary fig. S14, Supplementary Material online).

Discussion

We tested modes of population structuring in birds distributed across a biogeographic filter barrier, where we found that genomic landscapes were best explained by different geographic models across partitions at multiple scales. The disparity in predictors of intraspecific differentiation among the whole genome versus windows and between windows extends the view that evolutionary inferences are dependent on which portions of the genome are examined in a spatial framework. Despite this, individual species behave more consistently than expected across all of their corresponding genomic and phenotypic partitions. The heterogeneity in model fit between taxa partitions was consistent with the expectation that various evolutionary processes contribute to the peaks and valleys of the genomic landscape. By applying this framework across an assemblage of birds that evolved across a

common, dynamic region we showed that at the community scale, predictors of genomic structure remain idiosyncratic across the community, which may reflect taxa at different stages of the population histories and responses to a barrier that mediates gene flow.

Extrinsic Drivers of the Genomic Landscape

Our modeling showed that environmental distance was a common predictor of levels of intraspecific differentiation, but this pattern was species-dependent. Contemporary environment was the single most important or one of the most important factors in nearly 40% of partitions, followed closely by the paleoclimate environment (supplementary fig. S2, Supplementary Material online). Genome-wide patterns of differentiation across the Cochise Filter Barrier are partially shaped by environmental adaptation as observed in nonavian taxa distributed across the barrier (Myers et al. 2019). Environmental adaptation is often recovered in taxa who respond to environmental gradients via altered phenotypes (Branch et al. 2017; Dubuc-Messier et al. 2017), genotypes (Berg et al. 2015; Manthey and Moyle 2015), or both (Ribeiro et al. 2019). Despite the importance of environment on the genotype and phenotype in these birds, the fact that patterns are highly species specific instead suggests that individual taxa have unique responses to those environments. Although the focal taxa are co-distributed, we showed how environmental suitability, their general morphologies, and abundances across space varied among species, which may help explain why best-fit models differed. As such, these species-specific factors likely explain IBE was the best explanatory variable for many, but not all, of the species we investigated.

Individual partitions of the genome also varied with respect to how much environmental variation played a role. At one extreme, environmental variation appears to have a strong impact on the sex chromosomes. Environment was the most (or one of the most) important factor on the Z chromosome for 6/10 species, including species with population structure, a gradient, and panmixia. This is likely because the chromosome evolves faster than sites under selection for adaptation to local environmental conditions. Sex chromosomes are known to diverge faster than autosomes due to their differences in effective population size (Mank et al. 2010), importance in sexual selection (Kirkpatrick 2017), and the presence of speciation genes (Sæther et al. 2007). Given the evidence for environmental variation predicting genetic differentiation on the Z chromosome, this would suggest that any speciation genes present in these taxa may be involved in adaptation to the environment. The autosomes, in contrast to the sex chromosomes, vary in how important environment is, from some chromosomes with environment only being one of multiple factors (i.e., chromosome 1) to autosomes that are majority driven by environment (i.e., chromosome 27).

The environment was the most important driver for species with genetic structure, with 35.3% of partitions in structured species having the environment as the best model. The most intuitive explanation for this was that population structuring in these taxa was facilitated by natural selection to the environmental gradient across the barrier. There was some evidence that this could have happened across other taxa that occur across the Cochise Filter Barrier, as IBE was the best predictor of genome-wide divergence in a community of snakes distributed across the barrier (Myers et al. 2019). However, we must stress that while this explanation was the most intuitive and aligns with predictions, there are numerous processes that can produce IBE (Wang and Bradburd 2014), and it is possible that divergence led to adaptation to these environments secondarily, rather than the reverse, or the patterns are being influenced by some factors that we did not quantify. Nevertheless, at present, our results are consistent with the importance of ecologically mediated population differentiation, or IBE, in structuring communities across the deserts of North America.

Contemporary Versus Historical Predictors of Genomic Differentiation

Our finding that the best-fit models varied across species was consistent with the expectations that species idiosyncratically respond, over a range of time scales, to the Cochise Filter Barrier. The spatial patterns we examined vary temporally, with Pleistocene environmental changes being a historical process, while geographic distances, abundances, and environmental variation reflecting more contemporary processes. Historical signatures of Pleistocene isolation are commonly recovered patterns for the Cochise Filter Barrier (Provost et al. 2021) and other communities (Shafer et al. 2010; Ralston et al. 2021), and our data showed that isolation in glacial refugia best explained genome-wide differentiation in two of our species, one that showed a gradient of phylogeographic relatedness and one that was unstructured. Within chromosomes, there are two additional species where one of multiple, equally-well-fit predictors is historical isolation. The lack of signal in the other six species, particularly the ones with phylogeographic structure across the barrier, could be due to erosion of historical signals as the Cochise Filter Barrier filters taxa and changes the contemporary patterns of gene flow. Alternatively, our proxy for IBH (resistance over projected Pleistocene habitat suitability) may be a poor model for actual historical isolation. For example, paleoenvironmental gradients may no longer be as readily detectable. Nevertheless, this lack of support for paleoenvironmental factors, and thus glacial refugia, suggests that these processes may not leave strong detectable signals in the genomes of most of these desert birds.

In contrast, current environments best explain a large amount of genetic and morphological variation, suggesting that phenomena operating on more recent time scales influenced contemporary patterns across the landscape. If some of the taxa herein are going through incipient speciation, then these contemporary factors should be most potent. Our identification of species abundances as a relatively important predictor of genetic divergence aligns well with

landscape genetic studies that use proxies for the effects of contemporary phenomenon and ecological factors on genetic variation (Burney and Brumfield 2009; Paz et al. 2015). For example, urbanization, which fragments and reduces population sizes, is well known to impact rates of gene flow and drift, acting as a strong barrier of gene flow since the 20th century (Miles et al. 2019). Our use of available abundance data across large spatial scales shows a more direct relationship between varying abundances across the landscape with levels of differentiation. Furthermore, while both historical and contemporary processes are influencing taxa across this biogeographic barrier, environmental patterns in particular irrespective of timing seem more influential.

Relationship between Best-Models and Window Summary-Stats

In contrast to the extrinsic drivers of the genomic landscape that we have focused on here, there were few clear associations between partition characteristics and support for a particular model. For example, we found that regions with low predicted recombination rate were more likely to show multiple models as equally important. At the phylogeographic-scale, low recombination regions of the genome have been shown to be more likely to reflect population structure (Martin and Jiggins 2017; Manthey et al. 2021). The avian recombination rate landscape is thought to be conserved across taxa, even though exact genomic locations of divergence across taxa are not (Singhal et al. 2015; Turbek et al. 2021). Correlations in recombination rates at the same genomic position in other species are greater than 0.37 across chromosomes and always positive (Turbek et al. 2021), even across large phylogenetic distances. The ten desert birds we investigated, which range in divergence time from ~9 to ~55 million years between taxa (Mason and Burns 2013; Pasquet et al. 2014; Price et al. 2014; Barker et al. 2015; Gibb et al. 2015; Mitchell et al. 2016; Hooper and Price 2017; Kumar et al. 2017; Harris et al. 2018), have correlations in recombination rates at the same genomic position that were often smaller in magnitude and negative. This could reflect a real pattern, where the recombination landscapes are only conserved within more closely related species; our closest taxa, the two nonsister *Toxostoma*, do have the highest correlation in recombination rates across windows and are in the top 25% of the distribution in correlations. However, the differences found could have been caused by coverage depth, differences in the recombination rate estimators used, missing data allowance, or the fact that software that estimates recombination rates do not currently exist that can handle genotype likelihood data. In addition, genetic partitions with higher F_{ST} were more likely to show multiple best models as being important. We expect regions with high differentiation to instead be associated with the presence of the barrier if the barrier reflects actual divergence. However, this was not the case. We suggest that this reflects the gradient in differentiation across species in the community, both in the degree to which divergence has happened, the genomic locations of any differentiation, and the timing of divergence.

We explored the signal in our data by examining multiple ways of partitioning genomic windows, using different thresholds of missing data, and evaluating how data attributes influenced model support. We found that genetic partitions with more missing data were more likely to have ambiguous results. Genetic summary methods like PCA are impacted by missing data, particularly when they are imputed, which can cause individuals with disproportionately high levels of missing data to appear like they are admixed between populations (Yi and Latch 2022). It is likely that the reverse is true, where individuals with disproportionately low levels of missing data should fall out as their own populations more readily. Here, we expect individuals with exceptionally low coverage should behave similarly. For example, in some of our species (namely *Vireo bellii*, *Auriparus flaviceps*, *Polioptila melanura*), the individuals with highest missing data clustered as their own population before detecting any other spatial patterning. We ameliorated this by dropping individuals with too much missing data in some of our datasets. Overall, we did not find qualitative differences in population assignments, but it did generally inflate our fixation values and deflate our genetic diversity values. This is sensible, as reducing the number of individuals should both increase the likelihood of fixation due to sampling error as well as decrease the overall amount of nucleotide diversity.

The clines of population differentiation across space that we measured were narrower in longer chromosomes. One explanation for this is that larger chromosomes are more dense with respect to polymorphisms across the deserts (supplementary fig. S24, Supplementary Material online), therefore having more information content with respect to clines. However, we propose that this is mediated by recombination variation across the genome. Chromosome length is frequently negatively correlated with recombination rate, where generally, the recombination rates are lower on larger chromosomes due to the necessity of crossovers to ensure successful meiosis (Tigano et al. 2022). This is a common occurrence in many taxonomic groups (Kaback et al. 1992; Jensen-Seaman et al. 2004; Pessia et al. 2012; Farré et al. 2013; Kawakami et al. 2014; Haenel et al. 2018; Tigano et al. 2022). Lowered recombination rate would be less likely to break up genetic variants within the genome in the event of gene flow between two populations. Furthermore, SNP diversity is positively correlated with recombination, possibly due to mutagenesis at those sites (Lercher and Hurst 2002; Arbeithuber et al. 2015) Regions of low recombination are known to facilitate genomic changes such as selective sweeps (e.g., Burri et al. 2015; Bourgeois et al. 2019). However, in our dataset, recombination rate was not associated with the size of the chromosome. Post-hoc, we broke down this relationship into structured and unstructured species, where we found that species with structure or a gradient showed no association, while species that were panmictic exhibited the assumed negative relationship. Our within-species recombination estimating method is known to be sensitive

to historical demographic events (Adrion et al. 2020); as such, the presence of population structure herein may have caused the estimates to deviate from expected patterns. As such, we suspect that recombination landscape differences associated with chromosome length are contributing to the differences in these clinal patterns.

Morphological Versus Genetic Associations

We found that in most taxa, genotypic and phenotypic variation within species, and even different aspects of morphological phenotype within species, were not associated with the same landscape factors, in contrast to high congruence within species in different genotypic datasets. Phenotypes were better explained by abundance, whereas genotypes were better explained by the contemporary and historical environment. Discordance between genetic and phenotypic predictors of spatial variation have been observed in other systems, where phenotypic variation was better explained by the environment (Moreira et al. 2020). This discordance could be due to polygenic traits, where genotype–phenotype associations may be mediated by multiple loci of small effect working in concert, either by changing protein structure or regulation (Knief et al. 2017; Duntsch et al. 2020; Yusuf et al. 2020; Aguillon et al. 2021). However, for some phenotypes like plumage color, single genes of large effect have been implicated which should strengthen correlations between genotype and phenotype, at least for those loci (Toews et al. 2016; Sin et al. 2020). For desert birds in particular, phenotypic variation in metabolism (as well as in microbiomes) has been linked to genes that vary with the environment (Ribeiro et al. 2019). In our study, as with genetic differentiation, the extent of phenotypic structuring varied across species, with bill and body size being significantly different between deserts in a few taxa, but somewhat surprisingly, environmental variation did not usually explain morphological differences. For example, adaptations in bill morphology are frequently observed, such as in Song Sparrows on the Channel Islands that have higher bill surface area in hotter climates (Gamboa et al. 2021). The lack of a tight correlation between environment and phenotype in our study were likely reflective of the shallowness of the evolutionary divergences and the subtlety of the environmental gradient across deserts. The two *Toxostoma* species in our study have previously shown contrasting patterns with respect to climate on beak morphology: *T. crissale* has larger bills in drier habitats, which may aid in cooling while conserving water, while *T. curvirostre* showed a pattern contrary to thermoregulatory predictions with larger bills in cooler climates (Probst et al. 2022), suggesting even in closely related species climate may not have the same role on morphological variation. Even though phenotypic data partitions often did not have the same explanatory factor with respect to the general dissimilarity modeling, there was a correlation between population structure in the genome (and chromosomes to a lesser extent) and phenotypic variation across these ten birds, in that taxa lacking morphological change also lacked genetic variation overall.

Fitness Effects of the Cochise Filter Barrier

We found multiple species that have relatively sharp clines across the Cochise Filter Barrier, typically the taxa that also show population structure. These clines may represent areas that are hybrid zones, potentially under selection against the two populations coming back into contact. Our sampling throughout that transition zone is quite extensive, with the exception of *V. bellii*. In three species (*T. crissale*, *T. curvirostre*, and *M. fusca*), there are one or two individuals close to the transition zone between the deserts that have intermediate assignments between populations according to our NGSadmix analysis. For *T. curvirostre* in particular, this is close to where hybrid individuals have already been suggested to exist (e.g., Zink and Blackwell-Rago 2000). Furthermore, one species (*P. melanura*) has individuals close to this transition zone, though only when three populations are assigned rather than two. Multiple individuals of two species (*A. bilineata* and *C. sinuatus*) also come out as being admixed, but distributed throughout the range of the species. It is likely that the Cochise Filter Barrier is thus causing fitness effects, especially in those taxa that have few individuals admixed in the transition zone. Further investigation with more explicit determination of hybrid status in these species is likely warranted.

Conclusion

By quantifying patterns in genotypic and phenotypic variation in communities distributed across a barrier to gene flow, we found that multiple co-occurring processes occur that impact genomic and phenotypic divergence within taxa. Environmental gradients were among the most important associations in predicting genetic and phenotypic variation, but the best-fit model was highly associated with species-specific patterns. These findings underscore the importance of accounting for heterogeneity in the genome, phenome, and diversification mechanisms acting across time and space to have the most comprehensive picture of geographic structuring in species. This will allow for an assessment of whether biotic and abiotic geographic variation, which act as proxies for neutral and adaptive processes, consistently predict variation across phenotypes and genotypes that are evolving under the same conditions. Without a holistic understanding at each of these levels of organization, as well as the addition of future work that concurrently estimates selection at the organismal and the nucleotide levels, the actual mechanisms that shape communities will remain obscured. Overall, this work displays the necessity of integrating geographic predictors of population divergence, differentiation across the genomic landscape, and phenotypic variation in understanding the multiple different mechanisms that have produced the population histories we see across contemporary communities of birds in North America.

Methods and Materials

Study System

The Sonoran and Chihuahuan Deserts contain environmental and landscape variation that make them suitable for testing if any of the five discussed geographic models (IBA, IBB, IBD, IBE, and IBH) structure intraspecific variation in taxa. Across the two deserts and the transition zone between them, there is variation in precipitation, elevation, temperature, and vegetation that could result in local adaptation and IBE (Shreve 1942; Reynolds et al. 2004). Pleistocene glacial cycles repeatedly separated and connected, such that some taxa experienced dramatic range shifts (Smith et al. 2011; Zink 2014), which could have isolated taxa in each desert. Furthermore, there is a well-studied biogeographic barrier separating the deserts, the Cochise Filter Barrier, which is an environmental disjunction that demarcates the transition between the Sonoran and Chihuahuan Deserts of southwestern USA and northern Mexico. The barrier is thought to have begun forming during the Oligo-Miocene and completed during the Plio-Pleistocene (Morafka 1977; Van Devender et al. 1984; Van Devender 1990; Spencer 1996; Holmgren et al. 2007) and has formed a community ranging from highly differentiated taxa to unstructured populations (Provost et al. 2021). Demographic troughs caused by geographically varying population abundances could impact the frequency of gene flow across the landscape and the degree of genetic connectivity across the deserts.

Genetic Sequencing and Genome Processing

We performed whole-genome-resequencing for ten species of birds from the Sonoran and Chihuahuan Deserts, obtaining genetic samples from new expeditions and loans from natural history museums (*Cardinalis sinuatus*; *Toxostoma crissale*, *Toxostoma curvirostre*; *Amphispiza bilineata*, *Melozone fusca*; *Polioptila melanura*; *Phainopepla nitens*; *Auriparus flaviceps*; *Campylorhynchus brunneicapillus*; *Vireo bellii*; supplementary table S5 and fig. S15, Supplementary Material online). These species reflect different songbird morphotypes and ecologies in the deserts (e.g., large- to small-bodied, insectivorous to granivorous, migratory to resident). Three of these species (*V. bellii*, *T. curvirostre*, and *M. fusca*) have shown evidence of structure across the Cochise Filter Barrier, while an additional three (*P. melanura*, *A. flaviceps*, and *C. brunneicapillus*) have shown evidence of no structure (Zink et al. 2001; Rojas-Soto et al. 2007; Teutimez 2012; Klicka et al. 2016; Smith et al. 2018). However, some of the taxa without structure at the Cochise Filter Barrier do have structure at other barriers (e.g., Vázquez-Miranda et al. 2022).

Using 221 individuals across our 10 focal species, we sequenced 8–14 individuals in both the Sonoran and Chihuahuan Deserts per species for a total of 18–25 samples per species. We extracted DNA using the MagAttract HMW DNA Kit (Qiagen); 33 of the samples were extracted using a Phenol-Chloroform protocol, but we switched to the former to improve extraction quality. Library preparation and sequencing was performed by RAPiD Genomics (Gainesville, FL) on an Illumina HiSeq X Ten PE150. All individuals sent on the same plate were sequenced across *N* lanes, where *N* is the number of samples divided by 20. We sent six plates which ranged from 20 to 96 individuals (some plates also contained individuals from other projects).

We mapped raw reads of each species to their phylogenetic closest available reference genomes (supplementary table S6, Supplementary Material online): notably, *A. bilineata* and *M. fusca* were mapped to the same genome, as were *C. brunneicapillus*, *T. crissale*, *T. curvirostre*, *P. melanura*, and *P. nitens* (see supplementary information, Supplementary Material online). Before mapping, we created pseudochromosomal assemblies of these genomes using Satsuma version 3.1.0 (Grabherr et al. 2010) by aligning to the *Taeniopygia guttata* genome (GCF_000151805.1), retaining pseudochromosomes with the prefix "PseudoNC". Hereafter, pseudochromosomes will be referred to as chromosomes.

We filtered our sequences with FastQ Screen version 0.14.0 (Wingett and Andrews 2018) to remove contamination by filtering out reads that mapped to PhiX and the following genomes: *Homo sapiens*, *Escherichia coli*, *Enterobacteriophage lambda*, and *Rhodobacter sphaeroides*. For more details on bioinformatics methods, see supplementary information, Supplementary Material online. In brief, we did the following: From our raw reads, we used a pipeline that produced genotype likelihoods using ANGSD version 0.929 (Korneliussen et al. 2014). We converted cleaned FastQ files to BAM using bwa version 0.7.15 (Li and Durbin 2009, 2010) and picard version 2.18.7-SNAPSHOT from the GATK pipeline (McKenna et al. 2010; DePristo et al. 2011; Van der Auwera et al. 2013). Next, we prepared the BAM files to be used in the ANGSD pipeline using samtools version 1.9-37 (Li et al. 2009; Li 2011), bamUtil version 1.0.14 (Jun et al. 2015), and GATK version 3.8-1-0 (McKenna et al. 2010). This methodology creates genotype likelihoods to account for uncertainty for low-coverage sequences.

We investigated the impact of missing data (due to low coverage) on our analyses using three thresholds for retaining sites: a complete dataset, in which all individuals were retained irrespective of missing data; a 75% dataset, in which individuals were only retained if they had less than 75% missing sites; and a 50% dataset, in which individuals were only retained if they had less than 50% missing sites. These different datasets were used for a suite of downstream analyses to assess the sensitivity of the results to individuals with missing data.

Evaluating Population Structure across the Cochise Filter Barrier

We characterized the degree of population structure across the whole genome and in individual chromosomes across the Cochise Filter Barrier in our focal species. First, we used a combination of PCAngsd in ANGSD (Meisner and Albrechtsen 2018) and NGSadmix (Skotte et al. 2013), to assign individuals to K clusters and estimate admixture proportions for each individual. We chose $K = 2$ to

evaluate whether there was structure across the Cochise Filter Barrier (though we visualized *K* values from two to three). Because of differences in coverage among individuals, we performed this for the complete, 75%, and 50% missing data datasets, but found that these values were largely congruent across the datasets, and so we only use the complete dataset for describing population structure (supplementary figs. S16–S18, Supplementary Material online). Second, we plotted PCAngsd individual population assignments over space using a cline analysis via the hzar version 0.2-5 R package (Derryberry et al. 2014) and custom scripts (modified from Burbrink et al. 2021). Analyses were conducted in R version 3.6.1 (R Core Team 2019). We did this to quantitatively evaluate the differences in population structure across chromosomes and in the genome more broadly. We thus were able to calculate the location and width of clines for the entire genome and each chromosome.

Complementing our genome-wide analyses, we ran local principal components analysis along the genome on the complete dataset using the R package lostruct version 0.0.0.9000 (Li and Ralph 2019). Different chromosomes showed different relationships between individuals with respect to predicted phylogeographic relatedness (see supplementary information, Supplementary Material online). Because of this, we wanted to cluster regions of the genome together that showed similar relationships between individuals in case specific evolutionary processes were causing this pattern. The lostruct method performs principal component analysis (PCA) on individual windows of the genome, then uses multidimensional scaling (MSDS) to summarize how similar the windows' principal component analyses are when dividing the genome. To accommodate genotype likelihoods in the method, we calculated covariance matrices using PCAngsd to describe the relationships between individuals, then fed those covariance matrices into the lostruct code. We extracted three subsets of outliers for each species, which we designated LS1, LS2, and LS3, and compared it to the remainder of the genome, representing nonoutliers.

Genomic Summary Statistics

We characterized genetic variation across each species' genome and partitions of the genome by calculating a suite of summary statistics and metrics. To quantify genetic differentiation within each species, we calculated pairwise genetic distances from the genotype likelihoods using NGSdist (Vieira et al. 2016), which served as the genetic distance matrices for our GDM models (see below). Neighbor-joining trees were calculated from these matrices to contrast genealogies across the genome. Genealogies across the genome were visualized by calculating pairwise and normalized Robinson–Foulds (RF) distances between all pairs of trees per species (Robinson and Foulds 1981). We also performed a sliding window D_{XY} analysis using the calcDxy R script included with ngsTools version 1.0.2 (Fumagalli et al. 2014), which gives site-wise D_{XY} values, and then averaged across windows. Windows were overlapping with a size of 100,000 base pairs and offset by 10,000 base pairs. Missing data were calculated using vcftools (Danecek et al. 2011). This was calculated per window, per chromosome, per genome, per site, and per individual.

Using ANGSD's realSFS function, we performed a sliding window F_{ST} analysis by converting SAF output from ANGSD to a site frequency spectrum for both desert populations in each species. Detailed settings can be found in the supplementary information, Supplementary Material online. We performed F_{ST} outlier analysis for our species using the calculated F_{ST} values. *Z*-scores for F_{ST} for each species were calculated using the formula $ZF_{ST} = (\text{observed}F_{ST} - \text{mean}F_{ST})/SDF_{ST}$. We split the genome into two different partitions based on these *z*-scores: F_{ST} peaks, for values of F_{ST} greater than five standard deviations above the mean (*z*-score > 5) and F_{ST} troughs for values of F_{ST} greater than five standard deviations below the mean (*z*-score < -5). We only report the F_{ST} peaks in the main manuscript: for F_{ST} troughs, see supplementary information, Supplementary Material online. We performed this outlier detection for the complete, 75%, and 50% missing datasets to assess if low coverage impacted our calls.

Recombination rates (in crossovers per base pair, c/bp) across the genome were estimated using the program ReLERNN (Adrion et al. 2020), assuming a mutation rate of 2.21×10^{-9} mutations per site per year (Nam et al. 2010) and a generation time of 1 year. This program combines simulation with a recurrent neural network to estimate the recombination rate on each chromosome in 100,000 bp windows. At present, ReLERNN does not support genotype likelihoods, so we used SNPs in VCF format. We called SNPs using ANGSD with the following parameters: a *P*-value of 0.01; using the frequency as a prior; removing sites with a minor allele frequency below 0.05; a minimum mapping quality of 20; a minimum base quality score of 20; SNPs only called at a posterior probability greater than 0.95; minimum of four individuals with SNP.

Morphological Data

We quantified morphological variation in our ten focal species to assess which of the geographic models best explain morphological variation across the landscape (see *Generalized Dissimilarity Matrix Models*). We measured 366 specimens (19–59 per species), excluding known females and known juveniles to account for any variation attributed to sex and age. Of those, 29 were also present in the genomic dataset, with 0–8 individuals per species.

We generated seven raw plus seven compound morphological measurements, which we designated as proxies for thermoregulation and dispersal, respectively (see supplementary information, Supplementary Material online). We reduced the dimensionality of the 14 morphological measurements using a PCA. We then calculated four distance matrices between individuals: one Euclidean distance matrix for all morphological variables, where we calculated the Euclidean distance between individuals among all raw and calculated measurements; and

three Euclidean distance matrices for the first three principal components, PC1, PC2, and PC3. We assessed whether there were differences in morphological PCA space between the Sonoran and Chihuahuan Desert populations in each species using DABEST tests in the dabestr package version 0.3.0 (fig. 6; supplementary figs. S19 and S20, Supplementary Material online; Ho et al. 2019). Note that this method does not give explicit significance values, instead it shows whether expected confidence intervals overlap zero (i.e., no difference between deserts) or not.

Isolation across the Landscape at Different Temporal Resolutions

We calculated IBD matrices by calculating the Euclidean geographic distance between the latitude/longitude pair of each specimen in R. We used the WGS84 projection for all data. These variables were somewhat correlated with one another, though less so after accounting for geographic distance (supplementary fig. S21, Supplementary Material online).

To produce data for the IBH model, we calculated environmental resistances in the LGM (~21,000 years ago) for each species. To do this, we created ecological niche models (ENMs) using 19 layers representing contemporary climate (WorldClim; Hijmans et al. 2005) at a resolution of 2.5 arcminutes. We used MaxEnt (Phillips et al. 2006), with ENMeval version 0.3.1 as a wrapper function for model selection (Muscarella et al. 2014). ENMeval optimizes MaxEnt models based on different sets of feature classes and regularization values (supplementary table S7, Supplementary Material online; see supplementary information, Supplementary Material online). The contemporary ENMs (see IBE section below) were then backprojected to the LGM using WorldClim paleoclimate data (Hijmans et al. 2005). We also backprojected to the Mid-Holocene, but contemporary and Mid-Holocene ENMs were highly correlated, so we excluded the Mid-Holocene values from downstream analyses. We then scaled the LGM suitability values to range between 0 and 1 and calculated resistances across the environment using the least cost path distance method in ResistanceGA version 4.0-14 (Peterman et al. 2014; Peterman 2018). Regions of high resistance are predicted to reflect poor habitat and be costly to traverse through. The ENMs were thresholded to equal sensitivity-specificity values for visualization (supplementary fig. S22, Supplementary Material online).

We approximated IBB by assigning individuals based on their location relative to the Cochise Filter Barrier (see supplementary information, Supplementary Material online). For proximity to the Cochise Filter Barrier, we assigned individuals to either Sonoran or Chihuahuan populations either based on the results of the $K = 2$ clustering analysis, if there was structure across longitudes, or according to a cutoff of longitude if there was no structure. We chose 108°W longitude as our cutoff—individuals west of this point were deemed Sonoran, and individuals east of this point were deemed Chihuahuan (but see Provost et al. 2021). In some cases, species with genetic breaks had some uncertainty due to unsampled areas or admixed individuals—we labeled these individuals as being unclear with respect to their desert assignment. Georeferencing on some morphological specimens was poor, but all except two specimens (see Results) were identified at least to county level if not to a specific locality. When localities were given, we georeferenced the specimens to the nearest latitude/longitude. Otherwise, we assigned individuals to the centroid of their state or county.

We independently tested IBE by using two datasets: contemporary environmental distance and resistance. For the environmental distances, we used the 19 WorldClim bioclimatic layers (see IBH section). For the latitude/longitude location of each specimen used in both the morphological and genomic analysis, we extracted the values on those WorldClim layers and then calculated the Euclidean distances in environmental space between specimens. This gave us an estimate of how different the environments were at each specimen's locality. For the environmental resistances, we created ENMs using the WorldClim layers, then added layers for soil properties, distance to water, terrain features, and vegetation, and occurrence data for the focal species (see supplementary information, Supplementary Material online). We then calculated resistances and thresholded as described above.

To assess IBA, which had a temporal scale of the last 50 years, we obtained abundance information from the Breeding Bird Survey (Pardieck et al. 2019). This dataset consists of replicated transects where individual birds are counted across the whole of the United States. The methodology for counting is standardized and covers multiple decades of observations, with our dataset comprising data from 1966 to 2018. We downloaded raw data for all points, then subsetted our data to our ten focal species. We averaged the number of individuals across years (though some points only had a single year). We then interpolated across points using inverse distance weighted interpolation in the spatstat version 2.1-0 package in R ($idp = 5$). The interpolations were converted to rasters with extents and resolutions matching those of the ENMs. We then calculated resistances such that regions of high abundance had low resistance, to generate an abundance distance matrix between individuals.

Generalized Dissimilarity Matrix Models

We assessed the relative effect of alternative geographic models on intraspecific variation in our focal species by building GDM models). As spatial layers representing our five models, we calculated geographic distances, abundance resistances, environmental distance and resistance, separation by barrier, and paleoenvironmental resistance between all individuals in each species. The models likely represent different temporal resolutions, from millions of years ago to the present-day configuration of the barrier. These predictors served as the input parameters for our GDMs and will be discussed in detail below. With our

numerous response matrices (four morphological matrices, three genome matrices for each missing data cutoff, 35 matrices for chromosomes, five matrices for the lostruct partitions, and six matrices for the F_{ST} outliers with missing data cutoffs) and our six predictor matrices (with two for IBE: environmental distance, environmental resistance), we generated GDM models using the gdm package version 1.3.11 in R (Manion et al. 2018). We tested which of IBA, IBB, IBD, IBE, IBH, or a combination best explained the variation in the response matrix (see below). Not all species had all chromosomes sequenced, and not all models converged: we have omitted those data. For each of the 45 response matrices per species, we built a univariate model where the genomic/chromosomal variable was predicted solely by one of the six predictor matrices. We also built models with combinations of two (bivariate) or three variables (trivariate), which we present in the supplementary information, Supplementary Material online. Furthermore, we present the GDM results for the chromosomes in the supplementary information, Supplementary Material online. We compared the models based on the highest percent deviance explained.

To identify any overarching patterns with respect to which model of landscape evolution best explained genetic diversity (supplementary fig. S23, Supplementary Material online), we calculated four summary statistics for each chromosome, each lostruct and F_{ST} outlier partition, and the genome as a whole. We tested whether genomic summary statistics on each chromosome (F_{ST}, D_{XY}, missing data, recombination rate) were correlated with explained percent deviance with an analysis of variance (ANOVA) test and a Tukey's honest significant difference test (Miller 1981; Chambers et al. 1992; Yandell 1997) using the stats v. 3.6.1 package in R. We did this for the complete dataset; for 75% and 50% missing data datasets, see supplementary information, Supplementary Material online. We also calculated linear models comparing the proportion of each model to species-wide estimates of habitat suitability across the barrier. For all significance tests, we used an alpha value 0.05. However, due to multiple model testing for the GDM analyses, we applied a Bonferroni correction for simultaneous testing of six univariate models, with a final corrected alpha value of 0.0083 as our cutoff for all GDM tests (Bonferroni 1936).

We evaluated whether the best-predictors of genomic landscapes varied across species and across partitions of the data using χ^2 tests of significance, via the chisq.test function in the stats package in R. For each, the expected distributions assuming no differences between species, partitions, or structure were calculated and compared to the observed distributions. χ^2 tests were performed both with and without Monte Carlo simulations ($N = 2{,}000$ simulations each repeated 1,000 times).

Supplementary Material

Supplementary data are available at *Molecular Biology and Evolution* online.

Acknowledgements

This work would not have been possible without generous specimen loans from DMNH (J. Woods), UWBM (R. Faucett, J. Klicka, S. Birks), UMMZ (J. Hinshaw, B. Benz), TCWC (G. Voelker), MSB (M. L. Campbell, M. Andersen, C. Witt, A. Johnson, J. McCullough), LSUMZ (D. Dittmann, F. Sheldon), CUMV (V. Rohwer, C. Dardia), and AMNH (P. Sweet, P. Capainolo, B. Bird, T. Trombone). We are grateful to numerous State and Federal Collection Permit officers, and many BLM managers (T. Schnell, S. Cooke, M. McCabe, J. Atkinson, M. Daehler, S. Torrez, D. Tersey). Thanks to staff at Dalquest Desert Research Station (N. Horner) and Indio Mountains Research Station (J. Johnson). We thank M. Ingala for illustrating the birds used in many of our figures and for helpful feedback. Helpful input comes from the Smith Lab, S. Simpson, L. Musher, D. Fletcher, F. Burbrink, L. Alter, D. Kelly, I. Overcast, A. Xue, M. Hickerson, M. Blair, P. Galante, R. Harbert, E. Sterling, A. Xue, and E. Myers., the Underrepresented Genders in Museum Ornithology group, and the B. Carstens lab. We also thank two anonymous reviewers for their helpful feedback. This work was funded by the AMNH Frank M. Chapman Fund, American Ornithological Society, Society of Systematic Biologists, RGGS Sydney Anderson Travel Award, AMNH Linda H. Gormezano Fund, and AMNH RGGS Graduate Fellowship. B.T.S. was supported by the National Science Foundation award DEB-1655736. K.L.P. was supported by the National Science Foundation award DEB-2016189.

Data Availability

These scripts used to perform these analyses are found at https://github.com/kaiyaprovost/GDM_paper/. All data used to perform analyses are available on Dryad (https://doi.org/10.5061/dryad.msbcc2g2).

References

R Core Team. 2019. *R: a language and environment for statistical computing, version 3.0.2*. Vienna: R Foundation for Statistical Computing; 2013.

Adrion JR, Galloway JG, Kern AD. 2020. Predicting the landscape of recombination using deep learning. *Mol Biol Evol*. **37**:1790–1808.

Aguillon SM, Fitzpatrick JW, Bowman R, Schoech SJ, Clark AG, Coop G, Chen N. 2017. Deconstructing isolation-by-distance: the genomic consequences of limited dispersal. *PLoS Genet*. **13**(8): e1006911.

Aguillon SM, Walsh J, Lovette IJ. 2021. Extensive hybridization reveals multiple coloration genes underlying a complex plumage phenotype. *Proc R Soc B*. **288**:20201805.

Arbeithuber B, Betancourt AJ, Ebner T, Tiemann-Boege I. 2015. Crossovers are associated with mutation and biased gene conversion at recombination hotspots. *Proc Natl Acad Sci*. **112**: 2109–2114.

Barker FK, Burns KJ, Klicka J, Lanyon SM, Lovette IJ. 2015. New insights into New World biogeography: an integrated view from the phylogeny of blackbirds, cardinals, sparrows, tanagers, warblers, and allies. *Auk Ornithol Adv*. **132**:333–348.

Barrowclough GF, Groth JG, Mertz LA, Gutierrez RJ. 2005. Genetic structure, introgression, and a narrow hybrid zone between northern and California spotted owls (*Strix occidentalis*). *Mol Ecol*. **14**:1109–1120.

Barton NH, Hewitt GM. 1981. Hybrid zones and speciation. *In*: Atchley WR, Woodruff DS, editors. *Evolution and speciation: Essays in Honor of M. J. D. White*. Cambridge, MA: Cambridge University Press. p. 109–145.

Benzer S. 1961. On the topography of the genetic fine structure. *Proc Natl Acad Sci USA*. **47**:403.

Berg PR, Jentoft S, Star B, Ring KH, Knutsen H, Lien S, Jakobsen KS, Andre C. 2015. Adaptation to low salinity promotes genomic divergence in Atlantic cod (*Gadus morhua* L.). *Genome Biol Evol*. **7**: 1644–1663.

Bonferroni C. 1936. Teoria statistica delle classi e calcolo delle probabilita. *Pubblicazioni del R Istituto Superiore di Scienze Economiche e Commericiali di Firenze*. **8**:3–62.

Bourgeois Y, Ruggiero RP, Manthey JD, Boissinot S. 2019. Recent secondary contacts, linked selection, and variable recombination rates shape genomic diversity in the model species *Anolis carolinensis*. *Genome Biol Evol*. **11**(7):2009–2022.

Branch CL, Jahner JP, Kozlovsky DY, Parchman TL, Pravosudov VV. 2017. Absence of population structure across elevational gradients despite large phenotypic variation in mountain chickadees (*Poecile gambeli*). *R Soc Open Sci*. **4**:170057.

Burbrink FT, Gehara M, McKelvy AD, Myers EA. 2021. Resolving spatial complexities of hybridization in the context of the gray zone of speciation in North American ratsnakes (*Pantherophis obsoletus* complex). *Evolution* **75**:260–277.

Burney CW, Brumfield RT. 2009. Ecology predicts levels of genetic differentiation in Neotropical birds. *Am Natural*. **174**(3):358–368.

Burri R, Nater A, Kawakami T, Mugal CF, Olason PI, Smeds L, Suh A, Dutoit L, Bureš S, Garamszegi LZ, *et al.* 2015. Linked selection and recombination rate variation drive the evolution of the genomic landscape of differentiation across the speciation continuum of *Ficedula* flycatchers. *Genome Res*. **25**(11):1656–1665.

Chambers JM, Freeny AE, Heiberger RM. 1992. Analysis of variance. In: Chambers JM Hastie TJ, editors. *Statistical models in S*. Pacific Grove, CA: Wadsworth and Brooks/Cole. p. 145–194.

Danecek P, Auton A, Abecasis G, Albers CA, Banks E, DePristo MA, Handsaker RE, Lunter G, Marth GT, Sherry ST, *et al.* 2011. The variant call format and VCFtools. *Bioinformatics* **27**:2156–2158.

DePristo MA, Banks E, Poplin R, Garimella KV, Maguire JR, Hartl C, Philippakis AA, Del Angel G, Rivas MA, Hanna M, *et al.* 2011. A framework for variation discovery and genotyping using next-generation DNA sequencing data. *Nat Genet*. **43**:491.

Derryberry EP, Derryberry GE, Maley JM, Brumfield RT. 2014. HZAR: hybrid zone analysis using an R software package. *Mol Ecol Resour*. **14**:652–663.

Dubuc-Messier G, Réale D, Perret P, Charmantier A. 2017. Environmental heterogeneity and population differences in blue tits personality traits. *Behav Ecol*. **28**:448–459.

Duntsch L, Tomotani BM, de Villemereuil P, Brekke P, Lee KD, Ewen JG, Santure AW. 2020. Polygenic basis for adaptive morphological variation in a threatened Aotearoa | New Zealand bird, the hihi (*Notiomystis cincta*). *Proc R Soc B*. **287**:20200948.

Ellegren H, Smeds L, Burri R, Olason PI, Backström N, Kawakami T, Künstner A, Mäkinen H, Nadachowska-Brzyska K, Qvarnström A, *et al.* 2012. The genomic landscape of species divergence in *Ficedula* flycatchers. *Nature* **491**:756–760.

Farré M, Micheletti D, Ruiz-Herrera A. 2013. Recombination rates and genomic shuffling in human and chimpanzee—a new twist in the chromosomal speciation theory. *Mol Biol Evol*. **30**(4): 853–864.

Fumagalli M, Vieira FG, Linderoth T, Nielsen R. 2014. Ngstools: methods for population genetics analyses from next-generation sequencing data. *Bioinformatics* **30**:1486–1487.

Gamboa MP, Ghalambor CK, Sillett TS, Morrison SA, Funk WC. 2021. Adaptive divergence in bill morphology and other thermoregulatory traits is facilitated by restricted gene flow in song sparrows on the California Channel Islands. *Mol Ecol* **31**:603–619.

Gibb GC, England R, Hartig G, McLenachan PA, Taylor-Smith BL, McComish BJ, Cooper A, Penny D. 2015. New Zealand Passerines help clarify the diversification of major songbird lineages during the Oligocene. *Genome Biol Evol*. **7**:2983–2995.

Grabherr MG, Russell P, Meyer M, Mauceli E, Alföldi J, Di Palma F, Lindblad-Toh K. 2010. Genome-wide synteny through highly sensitive sequence alignment: Satsuma. *Bioinformatics* **26**:1145–1151.

Haenel Q, Laurentino TG, Roesti M, Berner D. 2018. Meta-analysis of chromosome-scale crossover rate variation in eukaryotes and its significance to evolutionary genomics. *Mol Ecol*. **27**(11):2477–2497.

Harris RB, Alström P, Ödeen A, Leaché AD. 2018. Discordance between genomic divergence and phenotypic variation in a rapidly evolving avian genus (*Motacilla*). *Mol Phylogenet Evol*. **120**: 183–195.

Hewitt GM. 1989. The subdivision of species by hybrid zones. In: Otte D, Endler J, editors. *Speciation and its consequences*. Sunderland, MA: Sinauer Associates. p. 85–110.

Hijmans RJ, Cameron SE, Parra JL, Jones PG, Jarvis A. 2005. Very high resolution interpolated climate surfaces for global land areas. *Int J Climatol*. **25**:1965–1978.

Ho J, Tumkaya T, Aryal S, Choi H, Claridge-Chang A. 2019. Moving beyond P values: data analysis with estimation graphics. *Nat Methods*. **16**:565–566.

Hodgkinson A, Eyre-Walker A. 2011. Variation in the mutation rate across mammalian genomes. *Nat Rev Genet*. **12**:756–766.

Holmgren CA, Norris J, Betancourt JL. 2007. Inferences about winter temperatures and summer rains from the late Quaternary record of C4 perennial grasses and C3 desert shrubs in the northern Chihuahuan Desert. *J Quat Sci*. **22**:141–161.

Holt RD. 2009. Bringing the Hutchinsonian niche into the 21st century: ecological and evolutionary perspectives. *Proc Natl Acad Sci*. **106**:19659–19665.

Hooper DM, Price TD. 2017. Chromosomal inversion differences correlate with range overlap in passerine birds. *Nat Ecol Evol*. **1**: 1526–1534.

Jensen-Seaman MI, Furey TS, Payseur BA, Lu Y, Roskin KM, Chen CF, Thomas MA, Haussler D, Jacob HJ. 2004. Comparative recombination rates in the rat, mouse, and human genomes. *Genome Res*. **14**(4):528–538.

Johri P, Charlesworth B, Jensen JD. 2020. Toward an evolutionarily appropriate null model: jointly inferring demography and purifying selection. *Genetics* **215**(1):173–192.

Jun G, Wing MK, Abecasis GR, Kang HM. 2015. An efficient and scalable analysis framework for variant extraction and refinement from population-scale DNA sequence data. *Genome Res*. **25**: 918–925.

Kaback DB, Guacci V, Barber D, Mahon JW. 1992. Chromosome size-dependent control of meiotic recombination. *Science* **256**(5054): 228–232.

Kawakami T, Smeds L, Backström N, Husby A, Qvarnström A, Mugal CF, Olason P, Ellegren H. 2014. A high-density linkage map enables a second-generation collared flycatcher genome assembly and reveals the patterns of avian recombination rate variation and chromosomal evolution. *Mol Ecol*. **23**(16):4035–4058.

Kirkpatrick M. 2017. The evolution of genome structure by natural and sexual selection. *J Hered*. **108**:3–11.

Klicka LB, Kus BE, Burns KJ. 2016. Conservation genomics reveals multiple evolutionary units within Bell's Vireo (*Vireo bellii*). *Conserv Genet*. **17**:455–471.

Knief U, Schielzeth H, Backström N, Hemmrich-Stanisak G, Wittig M, Franke A, Griffith SC, Ellegren H, Kempenaers B, Forstmeier W. 2017. Association mapping of morphological traits in wild and captive zebra finches: reliable within, but not between populations. *Mol Ecol*. **26**:1285–1305.

Korneliussen TS, Albrechtsen A, Nielsen R. 2014. ANGSD: analysis of next generation sequencing data. *BMC Bioinf.* **15**:356.

Kumar S, Stecher G, Suleski M, Hedges SB. 2017. Timetree: a resource for timelines, timetrees, and divergence times. *Mol Biol Evol*. **34**: 1812–1819.

Lercher MJ, Hurst LD. 2002. Human SNP variability and mutation rate are higher in regions of high recombination. *Trends Genet*. **18**:337–340.

Li H. 2011. A statistical framework for SNP calling, mutation discovery, association mapping and population genetical parameter estimation from sequencing data. *Bioinformatics* **27**:2987–2993.

Li H, Durbin R. 2009. Fast and accurate short read alignment with Burrows–Wheeler transform. *Bioinformatics* **25**:1754–1760.

Li H, Durbin R. 2010. Fast and accurate long-read alignment with Burrows–Wheeler transform. *Bioinformatics* **26**:589–595.

Li H, Handsaker B, Wysoker A, Fennell T, Ruan J, Homer N, Marth G, Abecasis G, Durbin R. 2009. The sequence alignment/map format and SAMtools. *Bioinformatics* **25**:2078–2079.

Li H, Ralph P. 2019. Local PCA shows how the effect of population structure differs along the genome. *Genetics* **211**:289–304.

Manion G, Lisk M, Ferrier S, Nieto-Lugilde D, Mokany K, Fitzpatrick MC. 2018. *Gdm: generalized dissimilarity modeling. R package version. 1(11)*.

Mank JE, Vicoso B, Berlin S, Charlesworth B. 2010. Effective population size and the Faster-X effect: empirical results and their interpretation. *Evolution* **64**:663–674.

Manthey JD, Klicka J, Spellman GM. 2021. The genomic signature of allopatric speciation in a songbird is shaped by genome architecture (Aves: *Certhia americana*). *Genome Biol Evol*. **13**(8):evab120.

Manthey JD, Moyle RG. 2015. Isolation by environment in White-breasted Nuthatches (*Sitta carolinensis*) of the Madrean Archipelago sky islands: a landscape genomics approach. *Mol Ecol*. **24**:3628–3638.

Martin SH, Jiggins CD. 2017. Interpreting the genomic landscape of introgression. *Curr Opin Genet Dev*. **47**:69–74.

Mason NA, Burns KJ. 2013. Molecular phylogenetics of the Neotropical seedeaters and seed-finches (*Sporophila*, *Oryzoborus*, *Dolospingus*). *Ornitol Neotrop*. **24**:139–155.

Mayr E. 1942. *Systematics and the origin of species, from the viewpoint of a zoologist*. New York: Columbia University Press.

McKenna A, Hanna M, Banks E, Sivachenko A, Cibulskis K, Kernytsky A, Garimella K, Altshuler D, Gabriel S, Daly M, *et al.* 2010. The Genome Analysis Toolkit: a MapReduce framework for analyzing next-generation DNA sequencing data. *Genome Res*. **20**(9): 1297–1303.

Meisner J, Albrechtsen A. 2018. Inferring population structure and admixture proportions in low-depth NGS data. *Genetics* **210**: 719–731.

Miles LS, Rivkin LR, Johnson MT, Munshi-South J, Verrelli BC. 2019. Gene flow and genetic drift in urban environments. *Mol Ecol*. **28**:4138–4151.

Miller RG. 1981. *Simultaneous statistical inference*. New York: Springer.

Mitchell KJ, Wood JR, Llamas B, McLenachan PA, Kardailsky O, Scofield RP, Worthy TH, Cooper A. 2016. Ancient mitochondrial genomes clarify the evolutionary history of New Zealand's enigmatic acanthisittid wrens. *Mol Phylogenet Evol*. **102**:295–304.

Morafka DJ. 1977. *A biogeographical analysis of the Chihuahuan Desert through its Herpetofauna*. Dordrecht: Springer.

Moreira LR, Hernandez-Baños BE, Smith BT. 2020. Spatial predictors of genomic and phenotypic variation differ in a lowland Middle American bird (*Icterus gularis*). *Mol Ecol*. **29**(16): 3084–3101.

Muscarella R, Galante PJ, Soley-Guardia M, Boria RA, Kass JM, Uriarte M, Anderson RP. 2014. ENM Eval: an R package for conducting spatially independent evaluations and estimating optimal model complexity for Maxent ecological niche models. *Methods Ecol Evol*. **5**:1198–1205.

Myers EA, Xue AT, Gehara M, Cox CL, Davis Rabosky AR, Lemos-Espinal J, Martínez-Gómez JE, Burbrink FT. 2019. Environmental heterogeneity and not vicariant biogeographic barriers generate community-wide population structure in desert-adapted snakes. *Mol Ecol*. **28**(20):4535–4548.

Nam K, Mugal C, Nabholz B, Schielzeth H, Wolf JB, Backström N, Künstner A, Balakrishnan CN, Heger A, Ponting CP, *et al.* 2010. Molecular evolution of genes in avian genomes. *Genome Biol*. **11**(6):1–7.

Nosil P, Schluter D. 2011. The genes underlying the process of speciation. *Trends Ecol Evol*. **26**:160–167.

Nuvoloni FM, Feres RJF, Gilbert B. 2016. Species turnover through time: colonization and extinction dynamics across metacommunities. *Am Natural*. **187**:786–796.

Pardieck KL, Ziolkowski Jr DJ, Lutmerding M, Aponte V, Hudson MA. 2019. *North American Breeding bird survey dataset 1966–2018, version 2018.0*. Laurel, MD: US Geological Survey, Patuxent Wildlife Research Center.

Pasquet E, Barker FK, Martens J, Tillier A, Cruaud C, Cibois A. 2014. Evolution within the nuthatches (Sittidae: Aves, Passeriformes): molecular phylogeny, biogeography, and ecological perspectives. *J Ornithol*. **155**:755–765.

Paz A, Ibáñez R, Lips KR, Crawford AJ. 2015. Testing the role of ecology and life history in structuring genetic variation across a landscape: a trait-based phylogeographic approach. *Mol Ecol*. **24**(14): 3723–3737.

Pessia E, Popa A, Mousset S, Rezvoy C, Duret L, Marais GA. 2012. Evidence for widespread GC-biased gene conversion in eukaryotes. *Genome Biol Evol*. **4**(7):675–682.

Peterman WE. 2018. ResistanceGA: an R package for the optimization of resistance surfaces using genetic algorithms. *Methods Ecol Evol*. **9**:1638–1647.

Peterman WE, Connette GM, Semlitsch RD, Eggert LS. 2014. Ecological resistance surfaces predict fine-scale genetic differentiation in a terrestrial woodland salamander. *Mol Ecol*. **23**: 2402–2413.

Phillips OL. 1996. Long-term environmental change in tropical forests: increasing tree turnover. *Environ Conserv*. **23**(3):235–248.

Phillips SJ, Anderson RP, Schapire RE. 2006. Maximum entropy modeling of species geographic distributions. *Ecol Model*. **190**:231–259.

Price TD, Hooper DM, Buchanan CD, Johansson US, Tietze DT, Alström P, Olsson U, Ghosh-Harihar M, Ishtiaq F, Gupta SK, *et al.* 2014. Niche filling slows the diversification of Himalayan songbirds. *Nature* **509**(7499):222–225.

Probst CM, Ralston J, Bentley I. 2022. Effects of climate on bill morphology within and across *Toxostoma* thrashers. *J Avian Biol* **2022**: e02871.

Provost KL, Myers EA, Smith BT. 2021. Community phylogeographic patterns reveal how a barrier filters and structures taxa in North American warm deserts. *J Biogeogr*. **48**:1267–1283.

Ralston J, FitzGerald AM, Burg TM, Starkloff NC, Warkentin IG, Kirchman JI. 2021. Comparative phylogeographic analysis suggests a shared history among eastern North American boreal forest birds. *Auk*. **138**(3):ukab018.

Relethford JH. 2004. Global patterns of isolation by distance based on genetic and morphological data. *Hum Biol*. **1**:499–513.

Reynolds JF, Kemp PR, Ogle K, Fernández RJ. 2004. Modifying the 'pulse-reserve' Paradigm for deserts of North America: precipitation pulses, soil water, and plant responses. *Oecologia* **141**: 194–210.

Ribeiro ÂM, Puetz L, Pattinson NB, Dalén L, Deng Y, Zhang G, da Fonseca RR, Smit B, Gilbert MTP. 2019. 31°South: the physiology of adaptation to arid conditions in a passerine bird. *Mol Ecol*. **28**(16):3709–3721.

Robinson DF, Foulds LR. 1981. Comparison of phylogenetic trees. *Math Biosci*. **53**:131–147.

Rojas-Soto OR, De Los Monteros AE, Zink RM. 2007. Phylogeography and patterns of differentiation in the curve-billed thrasher. *Condor* **109**:456–463.

Sexton JP, Hangartner SB, Hoffmann AA. 2014. Genetic isolation by environment or distance: which pattern of gene flow is most common? *Evolution* **68**(1):1–5.

Shafer AB, Cullingham CI, Cote SD, Coltman DW. 2010. Of glaciers and refugia: a decade of study sheds new light on the phylogeography of northwestern North America. *Mol Ecol*. **19**(21):4589–4621.
Shreve F. 1942. The desert vegetation of North America. *Bot Rev*. **8**: 195–246.
Sin SYW, Lu L, Edwards SV. 2020. De Novo assembly of the northern cardinal (*Cardinalis cardinalis*) genome reveals candidate regulatory regions for sexually dichromatic red plumage coloration. *G3: Genes|Genomes|Genetics* **10**(10):3541–3548.
Singhal S, Leffler EM, Sannareddy K, Turner I, Venn O, Hooper DM, Strand AI, Li Q, Raney B, Balakrishnan CN, *et al.* 2015. Stable recombination hotspots in birds. *Science* **350**(6263):928–932.
Skotte L, Korneliussen TS, Albrechtsen A. 2013. Estimating individual admixture proportions from next generation sequencing data. *Genetics* **195**(3):693–702.
Smith BT, Escalante P, Baños BEH, Navarro-Sigüenza AG, Rohwer S, Klicka J. 2011. The role of historical and contemporary processes on phylogeographic structure and genetic diversity in the Northern Cardinal, *Cardinalis cardinalis*. *BMC Evol Biol*. **11**:136.
Smith BT, Smith BT, Bryson Jr RW, Mauck III WM, Chaves J, Robbins MB, Aleixo A, Klicka J. 2018. Species delimitation and biogeography of the Gnatcatchers and Gnatwrens (Aves: Polioptilidae). *Mol Phylogenet Evol*. **126**: 45–57.
Spencer JE. 1996. Uplift of the Colorado Plateau due to lithosphere attenuation during Laramide low-angle subduction. *J Geophys Res Solid Earth*. **101**:13595–13609.
Sæther SA, Sætre GP, Borge T, Wiley C, Svedin N, Andersson G, Veen T, Haavie J, Servedio MR, Bures S, *et al.* 2007. Sex chromosome-linked species recognition and evolution of reproductive isolation in flycatchers. *Science* **318**:95–97.
Teutimez MR. 2012. *The cactus wren (Campylorhynchus brunneicapillus) in southern California: haplotype comparisons among coastal and inland populations*. Long Beach, CA: California State University.
Tigano A, Khan R, Omer AD, Weisz D, Dudchenko O, Multani AS, Pathak S, Behringer RR, Aiden EL, Fisher H, *et al.* 2022. Chromosome size affects sequence divergence between species through the interplay of recombination and selection. *Evolution* **76**(4):782–798.
Toews DP, Taylor SA, Vallender R, Brelsford A, Butcher BG, Messer PW, Lovette IJ. 2016. Plumage genes and little else distinguish the genomes of hybridizing warblers. *Curr Biol*. **26**:2313–2318.
Turbek SP, Browne M, Di Giacomo AS, Kopuchian C, Hochachka WM, Estalles C, Lijtmaer DA, Tubaro PL, Silveira LF, Lovette IJ, *et al.* 2021. Rapid speciation via the evolution of pre-mating isolation in the Iberá Seedeater. *Science* **371**(6536):1312–1312.
Van der Auwera GA, Carneiro MO, Hartl C, Poplin R, Del Angel G, Levy-Moonshine A, Jordan T, Shakir K, Roazen D, Thibault J, *et al.* 2013. From FastQ data to high-confidence variant calls: the genome analysis toolkit best practices pipeline. *Curr Protoc Bioinf*. **43**:11–10.
Van Devender TR. 1990. Late quaternary vegetation and climate of the Sonoran Desert, United States and Mexico. In: Betancourt JL Van Devender TR, Martin PS, editors. *Packrat middens: the last 40,000 years of biotic change*. Tucson, AZ: University of Arizona Press. p. 134–165.
Van Devender TR, Betancourt JL, Wimberly M. 1984. Biogeographic implications of a packrat midden sequence from the Sacramento Mountains, south-central New Mexico. *Quat Res*. **22**(3):344–360.
Vasconcellos MM, Colli GR, Weber JN, Ortiz EM, Rodrigues MT, Cannatella DC. 2019. Isolation by instability: historical climate change shapes population structure and genomic divergence of treefrogs in the Neotropical Cerrado savanna. *Mol Ecol*. **28**(7):1748–1764.
Vázquez-Miranda H, Zink RM, Pinto BJ. 2022. Comparative phylogenomic patterns in the Baja California avifauna, their conservation implications, and the stages in lineage divergence. *Mol Phylogenet Evol*. **171**:107466.
Vieira FG, Lassalle F, Korneliussen TS, Fumagalli M. 2016. Improving the estimation of genetic distances from Next-Generation Sequencing data. *Biol J Linnean Soc*. **117**(1):139–149.
Waldock C, Stuart-Smith RD, Albouy C, Cheung WW, Edgar GJ, Mouillot D, Tjiputra J, Pellissier L. 2022. A quantitative review of abundance-based species distribution models. *Ecography* **2022**: e05694.
Wang IJ, Bradburd GS. 2014. Isolation by environment. *Mol Ecol*. **23**: 5649–5662.
Wang J, Street NR, Park EJ, Liu J, Ingvarsson PK. 2020. Evidence for widespread selection in shaping the genomic landscape during speciation of *Populus*. *Mol Ecol*. **29**(6):1120–1136.
Weckworth BV, Musiani M, DeCesare NJ, McDevitt AD, Hebblewhite M, Mariani S. 2013. Preferred habitat and effective population size drive landscape genetic patterns in an endangered species. *Proc R Soc B Biol Sci*. **280**:20131756.
Wingett SW, Andrews S. 2018. Fastq Screen: a tool for multi-genome mapping and quality control. *F1000 Res*. **7**:1338.
Wright S. 1943. Isolation by distance. *Genetics* **28**(2):114.
Yandell BS. 1997. *Practical data analysis for designed experiments*. New York: Chapman & Hall/CRC.
Yi X, Latch EK. 2022. Nonrandom missing data can bias principal component analysis inference of population genetic structure. *Mol Ecol Resour*. **22**:602–611.
Yusuf L, Heatley MC, Palmer JP, Barton HJ, Cooney CR, Gossmann TI. 2020. Noncoding regions underpin avian bill shape diversification at macroevolutionary scales. *Genome Res*. **30**:553–565.
Zamudio KR, Bell RC, Mason NA. 2016. Phenotypes in phylogeography: species' traits, environmental variation, and vertebrate diversification. *Proc Natl Acad Sci*. **113**:8041–8048.
Zeng ZB. 1994. Precision mapping of quantitative trait loci. *Genetics* **136**(4):1457–1468.
Zink RM. 2014. Homage to Hutchinson, and the role of ecology in lineage divergence and speciation. *J Biogeogr*. **41**(5): 999–1006.
Zink RM, Blackwell-Rago RC. 2000. Species limits and recent population history in the Curve-billed Thrasher. *Condor* **102**(4): 881–886.
Zink RM, Kessen AE, Line TV, Blackwell-Rago RC. 2001. Comparative phylogeography of some aridland bird species. *Condor* **103**(1):1–10.